Efficient Color Artifact Removal Algorithm Based on High-Efficiency Video Coding (HEVC) for High-Dynamic Range Video Sequences

JONG-HYEOK LEE[1], YOUNG-WOON LEE[2], DONGSAN JUN[3], AND BYUNG-GYU KIM [ID][4], (Senior Member, IEEE)
[1]Research and Development Team, PIXTREE Inc., Seoul 08380, South Korea
[2]Department of Computer and Electronics Convergence Engineering, Sun Moon University, Asan 31460, South Korea
[3]Department of Information and Communication Engineering, Kyungnam University, Changwon 51767, South Korea
[4]Department of IT Engineering, Sookmyung Women's University, Seoul 04310, South Korea

Corresponding author: Byung-Gyu Kim (bg.kim@sookmyung.ac.kr)

ABSTRACT High efficiency video coding (HEVC) has been developed rapidly to support new generation display devices and their ultra high definition (UHD) with high dynamic range (HDR) and wide color gamut (WCG). To support HDR/WCG sequences on the HEVC standard, pre-/post-processing technique has been designed. After an HDR video is compressed, a reconstructed frame exhibits chromatic distortions that resemble color smearing. To remove this color artifact, we herein propose a block-level quantization parameter (QP) offset-control-based efficient compression algorithm for the HDR sequence. First, we extract the candidate coding units (CUs) with the annoying area to the human eye based on the just noticeable distortion (JND) model. Subsequently, the chromatic distorted blocks are verified by the activity function as the chromatic artifact is observed at the nearby strong edge. For the verified artifact blocks, we reassign the QPs for the Cb and Cr chroma components. Our experimental results show that the proposed method yields an average gain in BD-rate of 3.3% for U, and 3.4% for V with a negligible bitrate increase of 0.3% on average.

INDEX TERMS Color artifact, HDR/WCG, HEVC, perceptual artifact, quality improvement, video compression, adaptive QP control mechanism.

I. INTRODUCTION

Video compression technology is rapidly evolving with consumer's interest in high-quality content and technologies in various industries such as network and storage. The H.264/advanced video coding (AVC) that was produced with the support goal of maximum full high definition (HD) video (1920 × 1080 resolution) has emerged in 2004 [1]. To efficiently serve to UHD (i.e., 4k ~ 8k resolution), High Efficiency Video Coding (HEVC) has been developed by the Joint Collaboration Team on Video Coding (JCT-VC) with 50 % better compression efficiency than the H.264/AVC [2].

The HEVC has also been extended to support range extensions (RExt), scalability extensions (SHVC), and multiview extensions (MV-HEVC) as its second version [3]. The HEVC

The associate editor coordinating the review of this manuscript and approving it for publication was Yun Zhang [ID].

supports various video formats with high fidelity and high bit depth of more than 8 bits, and 4:2:2/4:4:4 color format from the extended HEVC second version.

Recently, the consumer's expectations for better quality-of-experience have increased significantly. Accordingly, contents with High Dynamic Range (HDR) and Wide Color Gamut (WCG) are used to provide realistic video service quality. The HDR and WCG allow the Human Visual System (HVS) to represent darker, brighter, and richer colors in a wider area than the traditional Standard Dynamic Range (SDR).

The dynamic range is defined as the ratio between the minimum and maximum luminance perceived or captured in a real scene or rendered by a display. Luminance is typically measured in candela (cd) per m^2, which is referred to as "nits". The sun has a luminance in the order of 6×10^8 nits, in blue sky in the morning, and 4,600 nits in the night sky, respectively.

The range of light energy during the day is vast and the light of the noonday sun can be as much as 10×10^9 more intense than that of starlight [4]. In a typical indoor scene, the luminance of the sky seen through a window is on the order of 10,000 nits, the luminance of a human face has almost 50 nits in the room, and a dark surface is approximately 1 nit in the room [5]. Therefore, the HDR is more suitable for approximating the capabilities of human vision than the SDR.

To support a realistic viewing experience for consumers, a WCG is applied as the second dimension. This implies an extension of the range of colors that are rendered or sensed. Color range is defined as a color gamut. The HDTV standard in CIE uses the 1931 xy-chromacity diagram prescribed by the BT.709 as a triangle [6], [7]. The UHDTV system is specified to be of a wider color gamut than HDTV and this color primary has been defined in BT.2020 [8]. Between the range of the BT.709 and BT.2020, the Pointer's gamut exists for real surface colors [9].

Contributions for the compression of SDR, HDR, and $360°$ video sequences have been reported in standardization group [10], and flexibility between different systems and suppliers is required to effectively commercialize new functions [11], [12]. In particular, the performance of image representation is important to support high bit-depths beyond the conventional 8-bit display.

To compress the HDR sequence, the HEVC has been updated to support a HDR and WCG by including the newest and most efficient coding tools [13]. HDR and WCG video coding have extended the format of the samples and color primaries are supported with a 10-bit integer, 16-bit floating point, 32-bit floating point, BT.709, BT.2020, and P3D65 respectively.

The conversion process has been adopted to compress the HDR video consisting of a half float 4:4:4 RGB linear-light format (e.g., OpenEXR) at the front and back from the encoding/decoding process. In the preprocessing stage, the input frame with a half float 4:4:4 RGB linear-light format (e.g. OpenEXR) is converted to a YUV frame with 4:2:0 10-bits using a conversion tool that call the HDRTools software.

The HEVC uses the YUV format, which is called as 4:2:0 10-bits as input to encode. The original input format is converted through color conversion, transform, quantization, and downsampling. The perceptual quantizer transfer function (PQ-TF) is used to convert RGB(float) to R'G'B'(float) in the coding TF stage. The PQ-TF is designed for mapping floating point HDR signal to 10-bit integer within just noticeable distortion (JND) of the human visual system (HVS). But 8-bit representation via this PQ mapping would introduce noticeable artifacts to human visual perception. The SDR represents the intensity range from 0.1 to 100 nits and the HDR has an intensity range from 0.0005 to 10,000 nits [14]. To reconstruct an image, the inverse process is performed to convert to RGB. With this structure, the HEVC can perform a successful tone mapping and efficient compression with the HDR sequence.

However, the HEVC with HDR sequences cause noise patches after encoding and subsequently in the decoding process. This color distortion renders it difficult to quantify the quantitative measurement of error and appears irregularly. In some works [15]–[20], it has been reported that this artifact was dominantly caused by the mosquito effect, motion compensation (MC) mismatch, blurring, and color bleeding. It has been reported that most of them were generated when the original data was encoded through video encoding system. This phenomenon occurs also when encoding the HDR sequences with the HEVC encoding standards. From this point, we can guess that the color bleeding or smearing results from the quantization to zero of the higher-order AC coefficients and thus resulting in the representation by only the lower-frequency basis images of the chrominance components. The problem is that this kind of color bleeding or smearing is very uncomfortable to human eye because of very uneven and frequent color changes. Therefore, it is necessary to remove the color bleedings or artifacts in the HDR video encoding stage, for providing more comfortable quality of the HDR video sequences.

In this paper, we herein propose a block-level quantization parameter (*QP*) offset-control-based efficient compression algorithm to remove this color artifact for the HDR sequence. To solve the occurrence of perceptual distortions, the proposed method classifies the offensive blocks of the HVS and predicts the occurrence of color artifacts like color bleeding. For the predicted block, to remove arbitrary and irregular color artifacts, we develop an adaptive block-level *QP* offset control algorithm on the HEVC encoding system.

The remainder of this paper is organized as follows. In Section II, we describe the color artifact and various approaches to solve it. In Section III, the proposed block-level *QP* offset control algorithm is described. The coding performance of the proposed algorithm is presented, discussed, and compared with the performance of other elimination methods for the color artifacts. In Section IV, the performance results of the proposed algorithm are discussed and compared with the HEVC anchor and those of other methods. Finally, the conclusion is presented in Section V. To remove color artifact, the Coding Units (CUs) with artifacts that are annoying to the human eye are classified as candidate blocks. These candidate blocks predict the block that contains color distortions such that it can be removed as perceptual artifact.

II. RELATED WORKS

Encoding/decoding process of HDR video on the HEVC can be represented as Fig. 1. When the HDR sequence is used to input the video coding system, unfortunately, chromatic distortions occurred in the reconstructed frame. In this section, the color artifact problem and the related approaches are discussed.

A. COLOR ARTIFACT

Perceptual artifacts are generated by video compression techniques because the bit rate of a coded sequence is a tradeoff
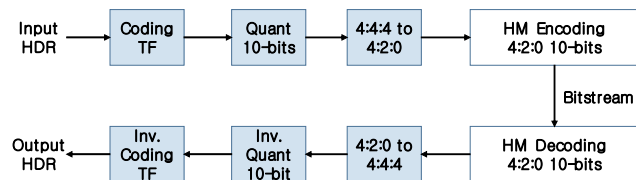
FIGURE 1. Structure of the HEVC encoding and decoding when HDR sequence is used as input.

with video quality degradation. Various types of artifacts are created by video coding schemes and have been studied previously [15]–[20].

Yuen and Wu [15] describe blocking effect, ringing, the mosquito effect, motion compensation (MC) mismatch, blurring, and color bleeding. They analyzed the spatial and temporal characteristics of video sequences that were susceptible to each artifact, and in which case the artifacts were visually prominent. Generally, the overall discussion relates to the hybrid MC/DPCM/DCT algorithm.

They mentioned the color bleeding effect as the blurring of the chrominance information. It results in the smearing of color between areas of strongly contrasting chrominance. Color bleeding results from the quantization to zero of the higher-order AC coefficients, thus resulting in the representation by only the lower-frequency basis images of the chrominance components.

The most interesting characteristic of the color artifact is that strong chrominance edges are accompanied by strong luminance edges. However, the existence of a strong luminance edge does not necessarily coincide with a strong chrominance edge [16]. Perceptual artifacts created by video compression have been summarized based on spatial and temporal, or reported in the previous study [17]. They have described that color bleeding was caused by inconsistencies across the luminance and chrominance channels. This artifact was often mentioned in video compression using the YCbCr 4:2:0 video format. Because a lower resolution was used in the chromatic channels, the rendering processes inevitably involve interpolation operations, leading to additional inconsistent color spreading in the rendering result.

In [18], color bleeding was also defined as color bleeding that results in a smearing of color between areas of strongly contrasting chrominance values. Meanwhile, in [19], it is defined as the significant smearing of color between areas of differing chrominance. Color bleeding occurred by two techniques in compression: subsampling of color components and quantization of images [20].

Therefore, color bleeding is caused by both the result of the coding/compression processes as well as the subsampling of the original source. Various types of distortions also appeared in the reconstructed frame after video encoding such as blurring, blocking, and ringing. These distortions are offensive noise that can be caused by annoyance during watching the video.

Fig. 2 shows an example of color bleeding. The reference frame is illustrated in Fig. 2(a) and a reconstructed frame is

FIGURE 2. Example of color bleeding in perceptual artifact [17]: (a) reference frame, (b) reconstructed frame.
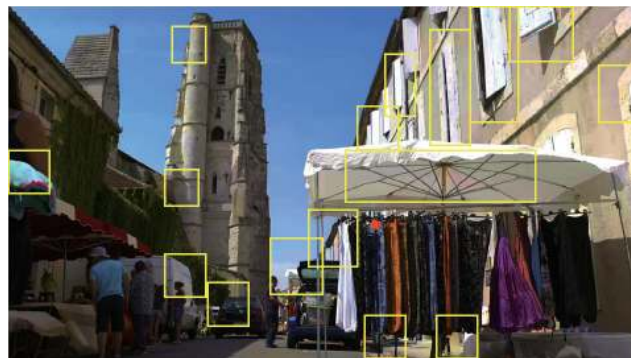

FIGURE 3. Color artifact occurring in images after compression on the HM 16.7 version for the reconstructed frame of S02 sequence by using $QP = 34$.

represented in Fig. 2(b) after video compression. In Fig. 2(b), the color artifact is represented as green patches near the boundary of bricks. Unfortunately, color bleeding is still an unsolved problem that affects the overall perceptual quality of the compressed video.

Fig. 3 shows the reconstructed frames coded by $QP = 34$ of Market3 as the HDR test sequence in the HEVC. Reconstructed frame exhibits chromatic distortions that resemble color patches of red/green, and pink/blue. We marked the color artifact with yellow boxes in Fig. 3. In the Market3 sequence, the chromatic distortion appears in white shutters, white canopy, and walls. We observed more perceptual artifacts when it was compressed into a lower bit rate environment in relation to the QP value.

FIGURE 4. Scaled color artifact images from Fig. 3 and other sequences.

Scaled images in Fig. 4 are from Fig. 3 and the other sequences. The perceptual artifact is clearly shown. Blue patches appear on the side of the white vehicle, the area between the white shutter door, walls, and the area around the garage door, as shown in Fig. 4. These patches of color bleeding make usually consumer's eye very fatigued while they are watching the decoded HDR video contents. Color artifacts after the HEVC encoding/decoding are problematic in rendering realistic video without annoying noise. Therefore, it is required to design more efficient and reliable color artifact elimination technique that can consider with encoding/decoding structure in the HDR video coding.

B. RECENT APPROACHES
To reduce color bleeding, post-processing techniques based on filtering have been proposed [21]–[24]. Spampinato *et al.* [21] have proposed a post-processing scheme to remove color bleeding using adaptive filtering in JPEG coding [22].

The primary steps consisted of edge detection, adaptive filtering, and fuzzy filter activation. In edge detection, the magnitude of each components for Y, Cb, and Cr is computed. Means of a 5×5 low pass filter (LPF) in both Cb and Cr channels are applied using an edge preserving weight and homogeneous weight for the chroma as the kernel taps. A final activation function is used to selectively filter only pixels that are representative of a chroma-only edge (likely affected by bleeding artifact).

Coudoux *et al.* [23] and Li *et al.* [24] proposed a color bleeding removal algorithm using the digital video compression technique. Li *et al.* [24] improved the visual quality by reducing color bleeding based on adaptive filtering in the H.264/AVC. The approaches mentioned above are based on filtering to improve a coded frame quality for the color bleeding, and were performed independently in both the encoder and decoder. Color bleeding was often found in the past, and occurred more severely in coded video frames. Particularly, color distortion is represented more in the display equipment for HDR contents.

To compress HDR content efficiently, various perception-based HDR compression algorithms have been proposed in [25]–[28]. Optimized bit-depth transformation and HVS

model based wavelet transform denoising have been proposed to provide efficient compression in terms of bitrate without compromising perceptual quality [25]. In [26], visual masking effect was studied to remove redundant imperceptible information for HDR content which could offer high levels of immersion. Intensity dependent spatial quantization method has been also proposed for perception-based HDR video compression [27], [28].

Recently, chromatic color artifact problems have been reported during the primary focus on HDR/WCG compression system, and researchers have observed that the chromatic artifacts increase when the bit rate decreases [29]. Thus, Taoran *et al.* [29] studied the phenomenon of color artifact generation in the existing HDR/WCG video coding and IPT-PQ color space. An adaptive reshaping has been proposed to improve both the color performance and texture details before and after the HEVC encoder/decoder using metadata.

Various quality enhancement algorithms have proposed to compensate HDR video as original input source on the HEVC [30]–[34]. The in-loop luma reshaper and luma based QP prediction have been proposed for HDR decoding in [30]. For HDR technology, color volume transform (CVT) has also been designed in pre-/post-processing in the HDR encoder and decoder [31]. In [32], luma adjustment has been proposed and luminance artifacts can be avoided. Additionally, an adaptive QP scheme and bit allocation between the chroma and luma by adjusting the chroma QP offset were proposed [33], [34]. This approach has been included and contributed in the recommended guidelines for the operation of the AVC or HEVC video coding system for compressing HDR/WCG video [10]. They has significantly increased the bits while improving the compressed image quality.

From the UHD sequence with HDR/WCG, a reconstructed frame with color artifacts as noise patches are generated after the HEVC encoding/decoding process despite applying the latest technology. However, noise did not occur unprecedentedly without video encoding stage. It means that the encoding and decoding process for the HDR sequences make color noise patches which is not appeared in the original video.

Although a sequence can be represented, patches of color bleeding bother consumers while they are watching it. In the HEVC, to remove the color artifact, their Cb and Cr QP offset values were signaled using the picture parameter set (PPS). The chroma QP offsets for the Cb and Cr models are denoted as following equations:

$$Offset_{Cb} = clip(round(C_{cb}(k \times QP + l)), -12, 0), \quad (1)$$
$$Offset_{Cr} = clip(round(C_{cr}(k \times QP + l)), -12, 0). \quad (2)$$

By the QP offset assignment, the color artifact can be significantly eliminated and the BDrates for the peak signal noise ratio (PSNR) of Y, U, and V are also improved significantly. However, the bit rate is significantly increased by applying the lower QP values for the Cb and Cr of all frames. Herein a new adaptive scheme is proposed to solve
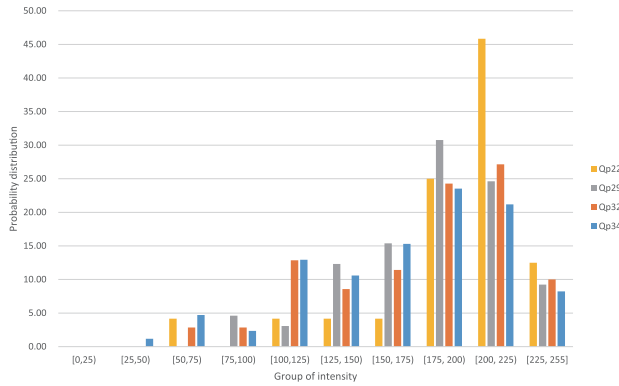
FIGURE 5. Probability distribution of relationship between intensity and color artifact occurring in Market3 sequence.

the problem of large bit increment for removing chromatic artifacts. The proposed scheme is based on the HVS and adaptive block-level detection to improve the visual quality for HDR sequences.

III. PROPOSED METHOD

This section describes an efficient video compression algorithm to remove chromatic distortions. The relationship between intensity and color artifact, and features related with the color artifact phenomenon are analyzed. Additionally, a new model is designed to eliminate chromatic distortions.

A. PERCEPTUAL OFFENSIVE BLOCK CLASSIFICATION

The color artifact is shown to be affected by an increased luminance level due to the adoption of the HDR technique. It is difficult to measure the amount of color bleeding areas exactly, and where they are generated in the block level. Thus, all of basic data for analysis and model design is made manually by human eye in respective test sequences such as Market3. Also, we observed similar distribution in some other sequences.

Fig. 5 shows the correlation between the brightness value of a frame of the Market3 sequence and the occurrence of the color artifact block in various QP values. The x-axis represents the intensity group, and the y-axis represents the probability distribution of the average luminance of the color artifact CU of size 64×64.

The color artifact has a high probability of generation in the block with a large intensity. Very little distribution occurs below the luminance value of 100, while the color artifact often occurs beyond the 100 value and reaches peaks between 200 and 225 when we divide the probability distribution into two classes with 125 brightness nearby mean value. Thus, the color artifact appears in a large value of luma and the relationship to various QP values appears to be low.

Tables 1 and 2 show the probability distributions of 10-bits and a normalized 8-bits of luminance from S02 Market3 sequence. These results consist of two groups of intensity as darkness and brightness range divided by the average value to derive a relationship between the luminance intensity and

TABLE 1. Summarized probability distribution by dividing from intensity value of 500 in 10-bits.

Group of intensity	$QP=22$ (%)	$QP=29$ (%)	$QP=32$ (%)	$QP=34$ (%)
[0, 500)	6.67	8.33	17.09	17.93
[500, 1023]	**93.33**	**91.67**	**82.91**	**82.07**

TABLE 2. Summarized probability distribution by dividing from intensity value of 125 in normalized 8-bits.

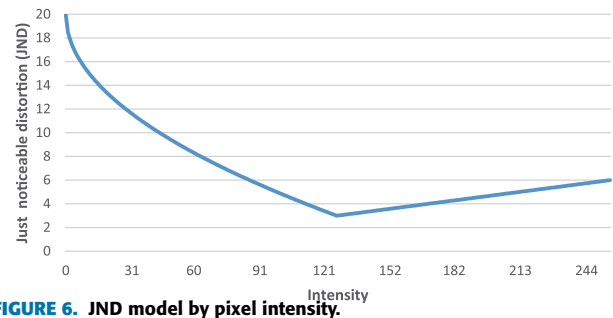| Group of intensity	$QP=22$ (%)	$QP=29$ (%)	$QP=32$ (%)	$QP=34$ (%)
[0, 125)	6.67	5.21	14.53	15.17
[125, 255]	**93.33**	**94.79**	**85.47**	**84.83**

FIGURE 6. JND model by pixel intensity.

color artifacts. For 10-bits signal as HEVC input format, darkness group achieved a probability distribution of least 6.67% up to 17.95%. However, results of bright area show high probability from 82.07% to 93.33% as different QP values. We can see that color artifacts arise at high rate of almost 87.5% on average in bright area and low probability of almost 12.51% in dark area.

Table 2 was measured by the normalized 8-bits from 10-bits of luminance. For the normalized 8-bits signal, the probability of artifact occurrence in bright area is high at about 90% on average. From this observation, the normalized 8-bits signal should be reasonable to decide whether the current coded block has color artifact or not. Thus, the normalized 8-bits signal may support the accuracy of the proposed artifact detection model.

Although the number of blocks in which color artifacts are less occurred in $QP = 22$ and more in $QP = 34$ in terms of total number of blocks with color artifact, the probability for occurrence of color artifacts in bright areas also can be seen low value because of the large quality degradation when $QP = 34$ as shown in Tables 1 and 2. From Tables 1 and 2, we can also observe high probability values of the occurrence of color artifact block at $QP = 22 \sim 29$, especially in bright intensity range.

The color artifact is unpleasant to the human eye during video watching. Because the color artifacts are sensitive to brightness and are visually irritating, techniques to efficiently capture and process them should be applied in video compression. Therefore, to capture these unpleasant areas to the eye in a compressed frame, a human vision system (HVS) is considered for the proposed technique.

The just noticeable distortion (JND) model is an important characteristic of the HVS, and expresses the visual stimulus

by the difference in brightness levels in the background. The JND function is used for improving subjective quality and various purposes in the video compression process [35]–[37]. The JND model is expressed as:

$$
JND(Y(i,j))
$$
$$
= \begin{cases} T_0 \times (1 - (Y(i,j)/127)^{\frac{1}{2}}) + 3, & \text{for } Y(i,j) \leq 127, \\ \gamma \times (Y(i,j) - 127) + 3, & \text{for } Y(i,j) > 127, \end{cases}
$$
$$(3)$$

where T_0, and γ are set to be 17, 3/128, respectively. $Y(i,j)$ means the intensity in the x and y of the pixel coordinates in an image. The JND model can calculate the human perceptual sensitivity according to the pixel intensity (in spatial domain). Based on the average brightness, the JND value of the current CU is denoted by (3). A lower value of the JND value means a more sensitive area in the frame in terms of the HVS.

A graphical representation of the JND model is shown in Fig. 6. From the average brightness of 127, the graph shows that the right side has a much higher stimulation rate in the luminance level, and the left graph region is the dark area. In addition, in the dark areas, the brightness is close to the average brightness, thus indicating high visual stimulation.

Figure 7 (a) and (b) represent the distribution for the JND values of the color artifact blocks. The Market3 (Fig. 7 (a)) and EBU_04_Hurdles (Fig. 7 (b)) sequences are used with four QP values of 22, 29, 32, and 34 as common test condition [39]. As shown in Fig. 7, the chromatic distortion occurs frequently in the high brightness range from 127 to the average value. It also has a high frequency for intensities between 86 to the average value in various QP values. Therefore, we define the condition to obtain the offensive block to perceptually satisfy the following equation:

$$
JND(CU) \leq Th_{JND}, \qquad (4)
$$

where Th_{JND} is a threshold value of 6 that contains the brightest value based on the JND model, in which it can be measured with the most sensitive area in the HVS. Using this equation, the coding blocks that have the highest sensitivity to the HVS and the color artifact can be classified using the JND model.

TABLE 3. Occupation ratio of the color artifact block by (4) in the reconstructed frames.

QP	Occupation ratio (%)
22	96.66
29	97.95
32	97.43
34	95.86
Avg.	96.98

Table 3 shows the experimental results when applying (4) to each QP value. From Table 3, we can determine the blocks that are most likely to affect the HVS, and where color artifacts are most likely to occur as candidate blocks. The proposed scheme only uses the normalized 8-bits signal from 10-bits of luminance to compose a candidate set.

B. ACTIVITIES FOR COLOR COMPONENTS

After the candidate blocks are filtered out with the JND model, we define the activity function of the current coding block to predict the chromatic distortions occurring in each color component. We design the activity model of the Cb and Cr color components based on the strong edge and disharmony between the color channels for the color artifact.

First, the proposed algorithm creates an edge map using the Sobel operator with the 3×3 masks. The gradient components at a pixel $I(x, y)$ are obtained by calculating the two weighted sums W_x and W_y in the x-dimension (vertical) and y-dimensions (horizontal), respectively. The gradient is computed with the weighted sums for the vertical and horizontal directions in (5) and (6).

$$
G_x(I(x, y)) = \sum_{i=-1}^{1} \sum_{j=-1}^{1} W_x(i, j) I(x+i, y+j), \qquad (5)
$$

$$
G_y(I(x, y)) = \sum_{i=-1}^{1} \sum_{j=-1}^{1} W_y(i, j) I(x+i, y+j), \qquad (6)
$$

where the weights $W_x(i, j)$ and $W_y(i, j)$ correspond to the elements of the Sobel mask $M_x(i+1, j+1)$ and $M_y(i+1, j+1)$, respectively. Equation (7) indicates the magnitude of gradient
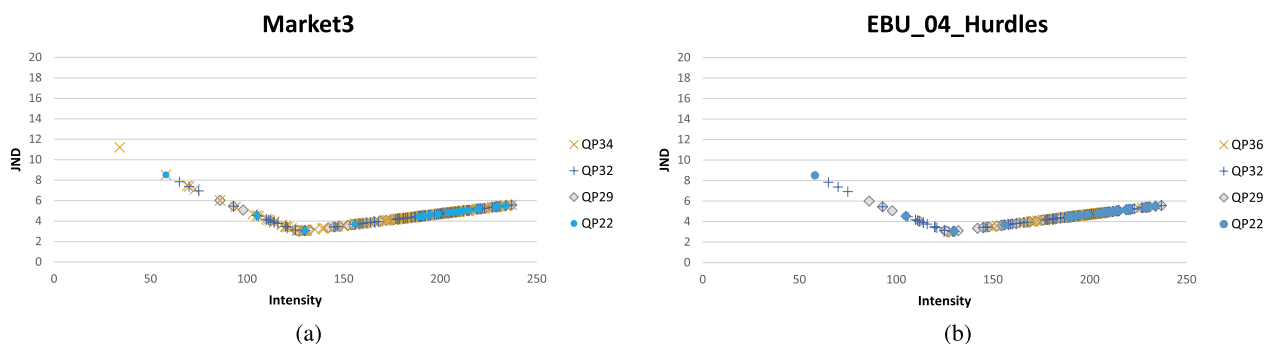

FIGURE 7. Distribution in the JND model according to block intensity of color artifact blocks.

TABLE 4. Performance of hit ratio for prediction of the color artifact in the CU satisfied *JND(CU)* in (4) using Th_{ACT} in (10).

	$Act(I_{Cb}^{CU})$	$Act(I_{Cr}^{CU})$	$Act(I_{Cb}^{CU})$ $\vee$ $Act(I_{Cr}^{CU})$
Hitratio	83.07	80	90.35

computed by using α as the weight factor that equal to 0.5.

$$G_{xy}(I_{cc}^t(x, y)) = \sum_{i=1}^{N} \sum_{j=1}^{M} \alpha \cdot G_x(I_{cc}^t(x+i, y+j))$$
$$+ (1 - \alpha)G_y(I_{cc}^t(x+i, y+j)). \quad (7)$$

The two weighted sums of (5) and (6) are calculated at each pixel of the current frame of the Cb and Cr component, respectively. Therefore, the gradient magnitude of each color component is calculated by gradient vectors $G_x(I_{cc})$ and $G_y(I_{cc})$. $I_{cc}^t(x, y)$ means pixel at position (x,y) about color component and block type of pixel area. Color component for Cb and Cr is represented as $cc \in \{Cb \text{ or } Cr\}$. A type includes the elements of frame, and the CU as the target image can be represented by $t \in \{Frame \text{ or } CU\}$.

To calculate the rate of change for the edge of the color component, (8) is calculated for the standard deviation of the gradient magnitude for a current coding block and its frame.

$$GradST(I_{cc}^t(x, y))$$
$$= \sqrt{\frac{1}{NM} \sum_{i=1}^{N} \sum_{j=1}^{M} (G_{xy}(I_{cc}^t(x+i, y+j)) - Gavg_{cc}^t)^2}, \quad (8)$$

where N and M are width and height of the frame or CU. G_{xy} is the magnitude of the gradient (7) and its average value denotes G_{avg}.

For CUs satisfied by the JND model in (4), the activity function is computed. It is designed to measure how the color space has changed, and to predict the color artifact occurring in an offensive block to the eye using the following equation:

$$\Delta Act(I_{cc}^{CU}) = \left| \frac{GradST(I_{cc}^{Frame}) - GradST(I_{cc}^{CU})}{GradST(I_{cc}^{Frame})} \right|, \quad (9)$$

where cc means the color components of chrominance channel as $cc \in \{Cb, Cr\}$. To predict the chromatic distortion of the CU, we define the condition as (10) using the activity model of the Cb and Cr component:

$$Act(I_{cc}^{CU}) \leq Th_{ACT}. \quad (10)$$

Table 4 shows the hit ratio of the activity function combined with the JND model. The activity model using the input Cb and Cr components of the CU classified by the JND model as (4) has sensitivity of 83.07% and 80%, respectively, when the activity is less than 0.6 of Th_{ACT}. We determined $Th_{ACT} = 0.6$ through experiment. When the activity of Cb and Cr are used together, the color artifact can be found as high as 90.5%. Equation (10) is satisfied when either $Act(I_{Cb}^{CU})$ or $Act(I_{Cr}^{CU})$ is true.
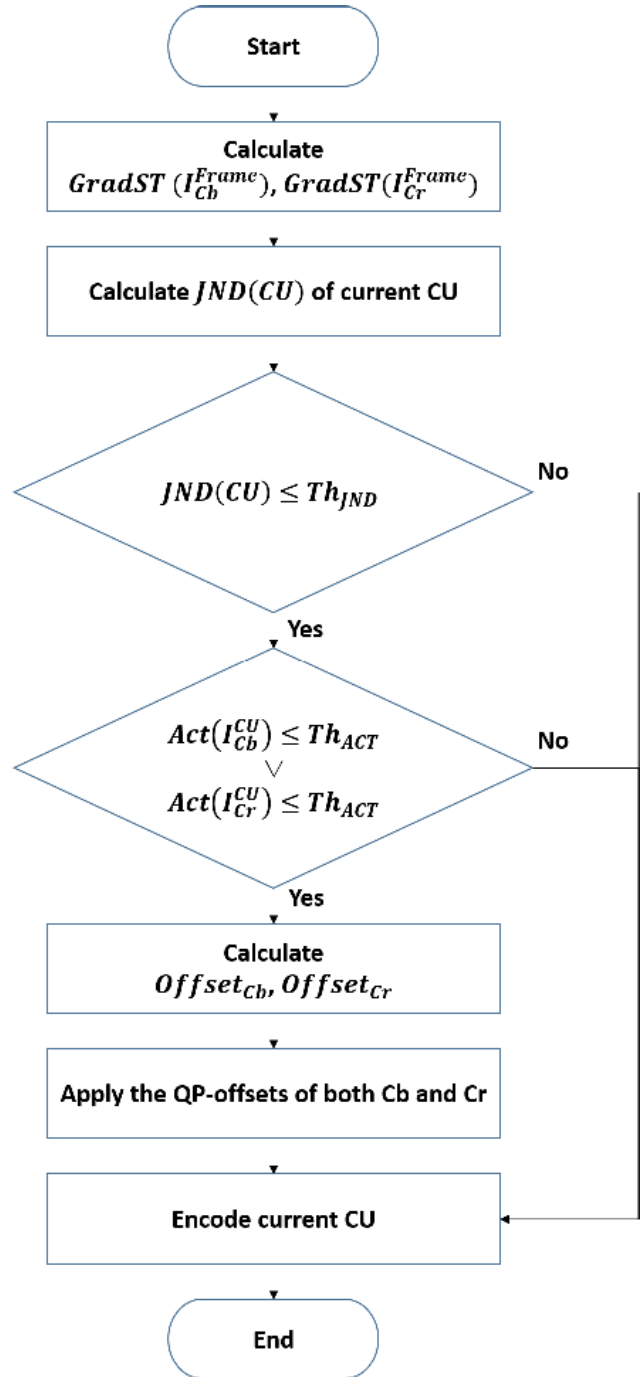

FIGURE 8. Overall procedure of the proposed color artifact removal algorithm.

Fig. 8 shows the overall flowchart of the proposed algorithm. To obtain the chromatic distortion block after encoding, the candidate blocks containing offensive characteristics to the human eye are first classified by the JND model. When the JND model is used, all the blocks are normalized to 8-bits. Regarding the annoying block, the variance of the gradient magnitude of each color space for the Cb or Cr component is used for the prediction by the phenomenon analysis of the color artifact. A color artifact block is expected if one of the

TABLE 5. Bitrate increase compared with the Anchor 3.2, the proposed method, and chroma *QP* offset [33].

Class		Sequences		Proposed method Δ bitrate (%)	[33] Δbitrate (%)
A	S00	FireEater		0.2	3.8
	S02	Market3		0.2	3.6
	S12	SunRise		0.3	2.2
B	S04	BikeSparklers	cut1	0.1	10.8
			cut2	0.3	6.8
	S13	GarageExit		0.4	4.4
C	S05	ShowGirl2Teaser		0.2	4.1
D	S06	StEM_MagicHour	cut1	0.5	4.2
			cut2	0.1	2.7
			cut3	0.2	4.2
	S07	StEM_WarmNight	cut1	0.1	2.4
			cut2	0.3	3.7
G	S08	BalloonFestival		1.0	7.6
H	S10	EBU_04_Hurdles		0.7	9.0
	S11	EBU_06_Start		0.5	11.4
		Average		**0.3**	**5.4**

TABLE 6. BDrate results of the proposed algorithm compared with Anchor 3.2.

Class		Sequences		PSNR Y(%)	PSNR U(%)	PSNR V(%)
A	S00	FireEater		0.1	-2.3	-3.3
	S02	Market3		0.0	-8.6	-7.2
	S12	SunRise		0.3	-4.2	-5.9
B	S04	BikeSparklers	cut1	0.2	-2.0	-2.3
			cut2	0.3	-1.7	-3.2
	S13	GarageExit		0.4	-2.2	-2.8
C	S05	ShowGirl2Teaser		0.0	-2.9	-1.5
D	S06	StEM_MagicHour	cut1	0.7	-3.5	-4.4
			cut2	0.1	-0.3	-1.2
			cut3	0.1	-0.2	-0.6
	S07	StEM_WarmNight	cut1	0.1	-2.7	-1.7
			cut2	0.3	-2.5	-1.7
G	S08	BalloonFestival		0.9	-5.8	-6.4
H	S10	EBU_04_Hurdles		0.5	-5.0	-4.7
	S11	EBU_06_Start		0.5	-5.2	-3.5
		Average		**0.3**	**-3.3**	**-3.4**

two color components of a coding block has increased the rate of change by more than a certain amount, based on (10).

Therefore, the proposed algorithm identifies visually irritating blocks by considering the HVS, and reduces the bit rate increase by applying the offset of the quantization parameters only to the blocks expected to generate color artifacts.

IV. EXPERIMENTAL RESULT

We implemented the proposed algorithm on the HEVC reference software HM version 16.7 as Anchor 3.2 [38]. The performance of the proposed method and chroma *QP* offset algorithm [33] was investigated. We verified that the proposed technique enhances the efficient coding performance of the current video codec. The evaluation was performed using test sequences with various *QP* values specified by the common test condition (CTC) for HDR/WCG video coding [39].

The tested sequences consist of six classes and successive cuts are included for S04, S06, and S07. The resolutions of the sequences are 1920 × 1080 progressive with RGB 4:4:4 format, and the color primaries of the content consist of either BT.2020 or P3 with D65 white point (P3D65) depending on the content. The original HM (Anchor 3.2) uses the chroma *QP* method [33] to remove the color artifact. The chroma *QP* offset algorithm has been reported to cause a significant bit rate increase.

Table 5 shows the increment of bit rate on Anchor 3.2 compared with the proposed algorithm and chroma *QP* offset [33]. The chroma *QP* offset method shows the performance of a minimum bit rate increase of 2.2 % and a maximum of 11.4%, while the proposed method achieved a negligible increase of 0.1% to 1.0%bit rate compared with Anchor 3.2. The average bit rate increments were 0.3% and 5.4% for the proposed algorithm and the chroma *QP* offset model, respectively. The chroma *QP* offset method shows a significant increase in the bit rate because offsets are applied to the entire frame using the PPS. However, the proposed

algorithm caused only small bit increments to improve the quality.

Table 6 shows the BDrate of Y, U, and V components of the proposed algorithm. The proposed method shows a 0.3 % of Y loss on average and a 3.3% of U and a 3.4% of V quality improvement. The BDrate has been achieved at least 0.1% to maximum 0.9% loss of Y, from 0.2%, and 8.6% better quality in U component. An improvement in quality is shown from a minimum of 0.6% to a maximum of 7.2% in V component.

Figure 9 shows the rate-distortion (R-D) curves of S00, S08, S10, and S13 sequences on the original HM 16.7 as Anchor 3.2, chroma *QP* offset [33], and the proposed algorithm. Figure 9(a) to 9(d) show rate-distortion curves for Y component. Rate-distortion curves of U and V components are represented from Fig. 9(e) to 9(h). The chroma *QP* offset method [33] shows a significant bitrate/quality degradation on $Y - PSNR$ in all the test sequences. Although the proposed algorithm has very small loss of bitrate compared with the Anchor 3.2 for tested sequences, we can observe that the proposed method gave better performance than the chroma *QP* offset method [33].

In terms of *U* and *V* components, the quality of the proposed method is lower than chroma *QP* offset method [33] while it is higher than Anchor 3.2. Other sequences achieved similar results in Fig. 9. The chroma *QP* offset method assigned assigned higher bits to preserve chrominance coefficient and achieved high $U - PSNR$ and $V - PSNR$ values. From the results, we can induce that the proposed scheme can eliminate chrominance artifacts efficiently even though additional bits less than chroma *QP* offset method are allocated.

For a very dark sequence such as S00 FireEater, the proposed algorithm also provided good quality when compared with the chroma *QP* offset method [33] as shown in Fig. 9(a). From results, we are able to see that the proposed model is reliable to remove the chrominance artifacts.

HDR-VQM is an objective quality estimator for HDR video [40]. A lower HDR-VQM score means a better quality of HDR video. Figure 10 shows the quality assessment
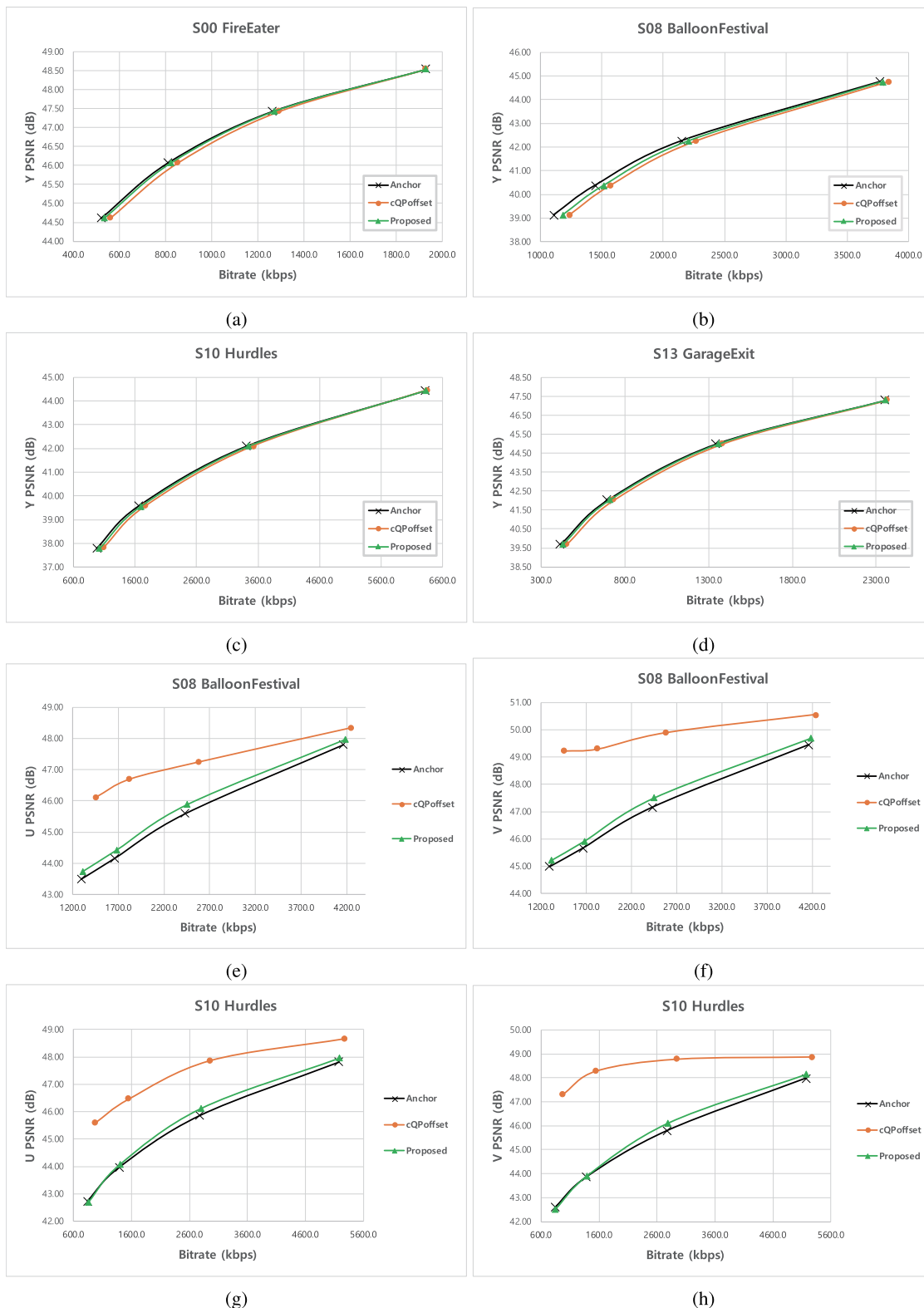
FIGURE 9. RD performance of the proposed method and chroma *QP* offset method (cQPoffset) [33] compare with the Anchor: (a) S00 FireEater, (b) S08 BalloonFestival, (c) S10 EBU 04 Hurdles, and (d) S13 GarageExit sequence for Y; Results for U and V component: S08 and S10 sequence in (e) to (h).

by the HDR-VQM about Market3 and StEM WarmNight cut1 sequences between Anchor 3.2 and the proposed algorithm. The proposed method achieves better performance for

HDR-VQM score in total sequences. As shown in Figs. 10 (a) and (b), the proposed algorithm is more efficient when bitrate factor is considered together.
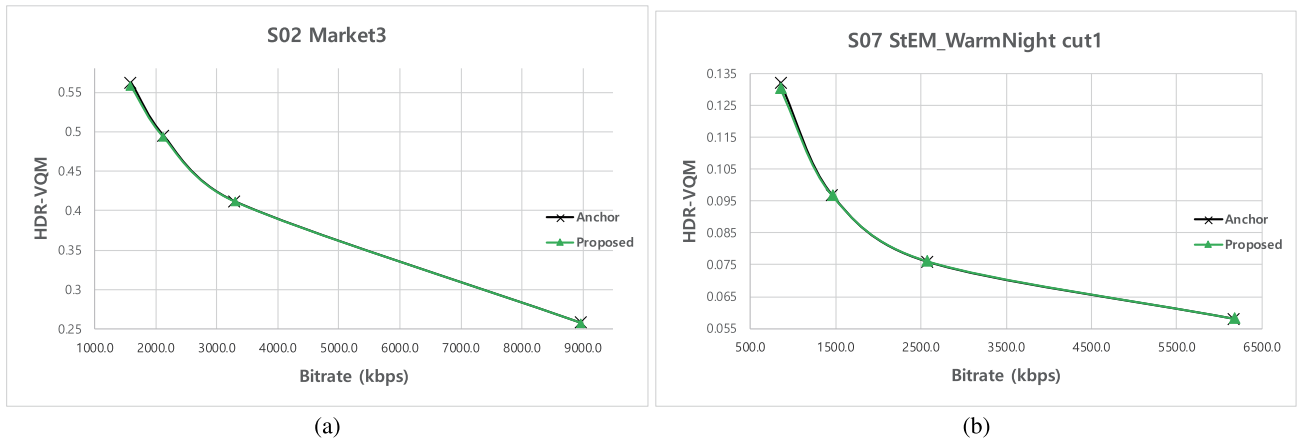
FIGURE 10. Result of quality assessment by HDR-VQM: (a) S02 Market3 and (b) S07 StEM WarmNight cut1 sequence.
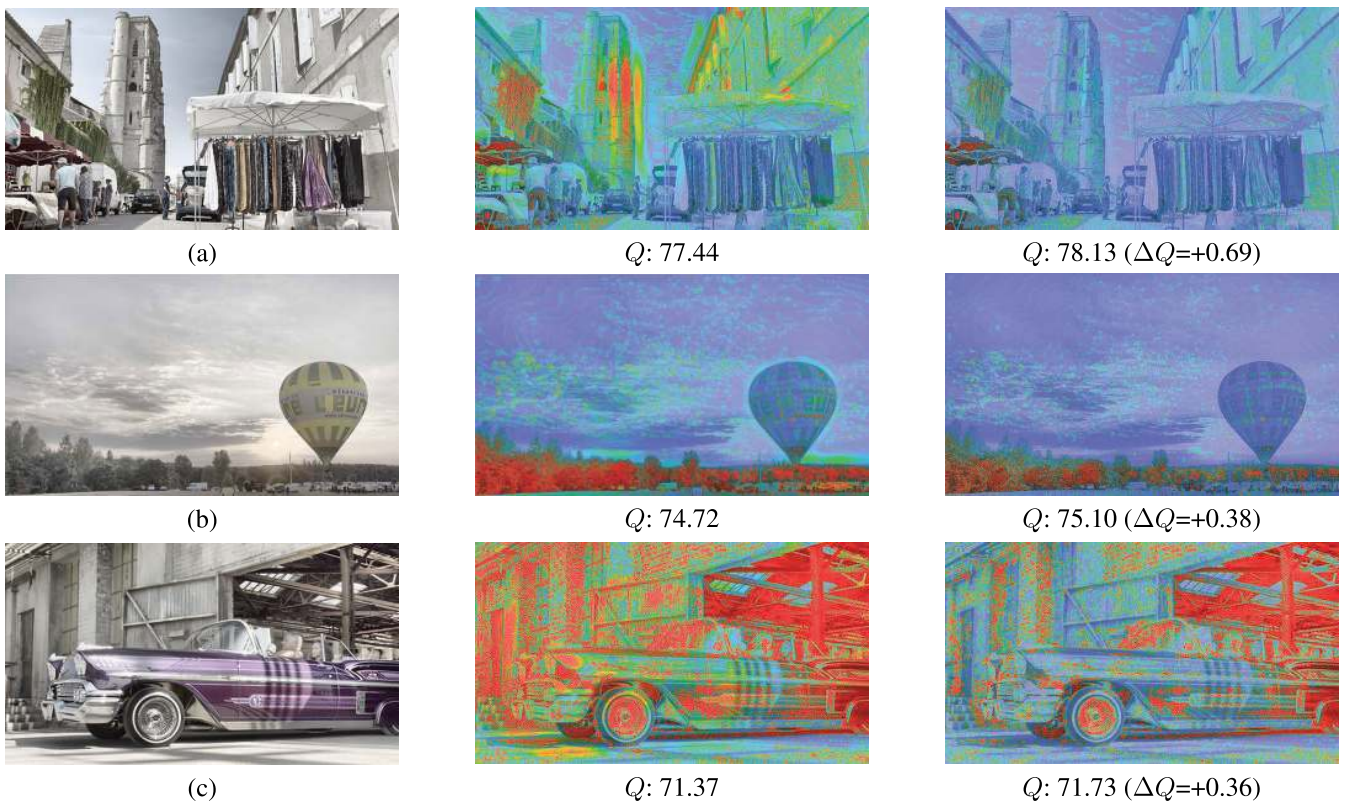

FIGURE 11. Visualization of the HDR-VDP-2 results for (a)Market3, (b)SunRise, and (c)GarageExit. *left:* the original reference frame, *center:* encoded frame by Anchor 3.2, *right:* encoded frame with the proposed color artifact removal algorithm.

To demonstrate the subjective quality improvement, the results of Mean Opinion Score (MOS) are evaluated by 30 observers in Table 7 and visual results are illustrated in Fig. 12. Subjective video quality assessment such as the MOS is used in the domain of Quality of Experience. It consists of inviting a group of subjects to judge the quality of a set of videos under well defined conditions by the International Telecommunication Union (ITU) [41]. As shown in Table 7, the MOS values of some sequences such as S04 cut1, S06 cut3, and S07 cut2 were evaluated as similar to the Anchor 3.2. However, for others, the results showed that the

compressed HDR sequences by the proposed method have been improved in terms of the quality of video.

To prove the improvement performance quantitatively, we employed the HDR-VDP-2 which is well known as a calibrated visual metric for visibility and quality predictions in all luminance conditions [42], [43]. Table 8 shows the HDR-VDP-2 measurements (Average Q values) for 7 test sequences. Each Q value (Anchor and the proposed) represents an average value of 30 frames and all QPs (22, 29, 32, 36) for each sequence. The Q value is a probabilistic indicator that how much the result of the applied method is close to the

TABLE 7. MOS results of the proposed algorithm compared with Anchor 3.2.

	Sequences		MOS value
S02	Market3		4.43
S04	BikeSparklers	cut1	3.1
		cut2	4.5
S06	StEM_MagicHour	cut2	3.83
		cut3	3.2
S07	StEM_WarmNight	cut1	4.5
		cut2	2.9
S10	EBU_04_Hurdles		3.93
S11	EBU_06_Start		4.4
S13	GarageExit		4.57

TABLE 8. HDR-VDP-2 Results (Average Q and ΔQ values, 30 frames, $QP = 22, 29, 32, 36$).

Sequences	Average Q value		Average ΔQ	Max. ΔQ
	Anchor 3.2	Proposed		
FireEater	68.9840	68.8966	+0.0026	+0.1158
Market3	75.1964	75.2152	+0.0187	+0.6914
BikeSparklers	71.7065	71.7265	+0.0200	+0.4289
BalloonFestival	77.2084	77.2459	+0.0375	+0.2735
EBU_04_ Hurdles	72.9295	72.9361	+0.0066	+0.2648
EBU_06_ Starting	73.4287	73.4597	+0.0310	+0.2667
GarageExit	71.4216	71.5404	+0.1188	+0.3632

original HDR image. It means that the lager value can give the better quality of the decoded image. From Table 8, we can see the positive average ΔQ values even though some values were very small in the average.

Also, we displayed some visualizations of the HDR-VDP-2 measurement. Figure 11 shows some visualized results. In the HDR-VDP-2, more blued color means it is closer to the original color. On the contrary, the more corrupted area is shown as the red color. Based on the original reference frame, the difference between the encoded frames are shown. It can be seen that the encoded frame by the proposed method

appears more blue, which is more likely to be closer to the original reference image. From these results, we are able to know that the proposed method can remove the critical artifacts that occur locally in the HDR image.

Figure 12 shows the results of the improvement in quality of the proposed algorithm by removing the color artifact for a compressed frame. In Fig. 12(a), the distortions of blue/cyan appear in the windows, white shutters, car, wall of building, and sky at sunrise. The improved images are shown in Fig. 12(b). The proposed algorithm provides better image quality by eliminating smearing color distortions. The removal of chromatic distortions is apparent in the white car, wall, windows, and sky at sunrise.
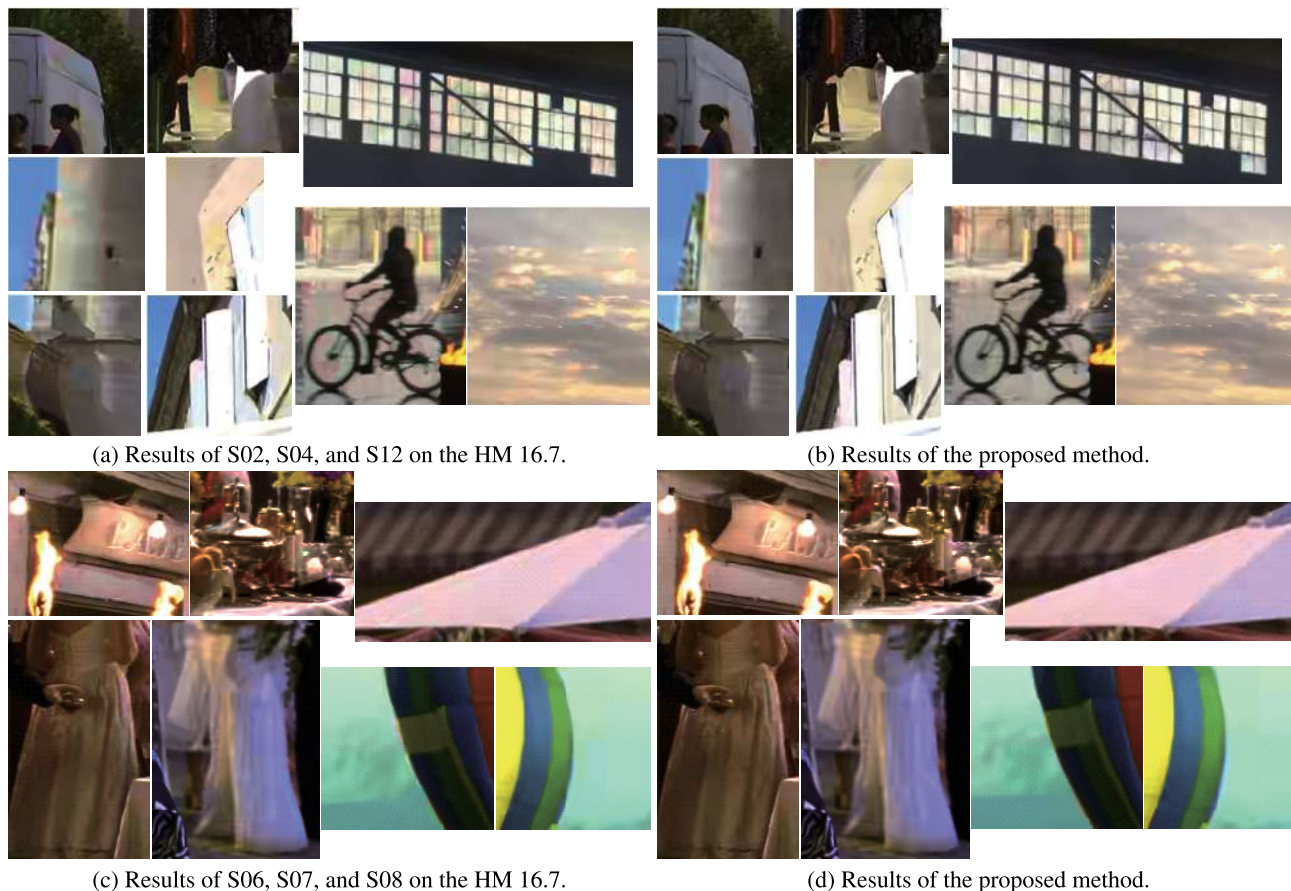

(a) Results of S02, S04, and S12 on the HM 16.7.

(b) Results of the proposed method.

(c) Results of S06, S07, and S08 on the HM 16.7.

(d) Results of the proposed method.

FIGURE 12. Eliminated images for the color artifact on the proposed algorithm: (a) and (c) are reconstructed images on the original HM 16.7 (Anchor 3.2); (b) and (d) indicate the removed color artifact results by the proposed algorithm.

As shown in Figs. 12(c) and (d), the color artifact elimination occurs at the sign and wall under the sign, shadow of the basket on the table, white dress, and pink umbrella. The proposed algorithm provides a clear effect of color artifact removal by preventing the disharmony of color components in the boundary edge of the object, as shown at boundary of the balloon in Figs. 12(c) and (d).

The suggested method also did not completely eliminate the color artifacts, as shown in the bicycle image (Fig. 12(a) and (b)), However, the proposed algorithm clearly improves the compressed video quality with little bit rate increment over the HEVC because of the proposed adaptive color artifact reduction. Therefore, the proposed method provides pleasant viewing results by eliminating annoying color distortions and has better frame clarity, and compression efficiency in terms of video coding.

V. CONCLUSION

We proposed an efficient algorithm to eliminate the color artifact for the HDR video sequence in video compression. To solve the occurrence of perceptual distortions, the proposed method classified the offensive blocks of the HVS and predicted the occurrence of color artifacts. For the predicted block, to remove arbitrary and irregular color artifacts, we designed an adaptive block-level QP offset control algorithm on the HEVC coding.

The proposed algorithm identifies visually irritating blocks by considering the HVS and reduced the bit rate increase by applying the offset of the QPs only to the blocks expected to generate color artifacts. The proposed method showed a quality improvement of 3.3% and 3.4% for U and V, respectively, with negligible bit rate increase. Therefore, the proposed algorithm provided efficient video compression with little increase in bit rate while eliminating color artifacts and improving quality.

REFERENCES

[1] T. Wiegand, G. J. Sullivan, G. Bjøntegaard, and A. Luthra, "Overview of the H.264/AVC video coding standard," *IEEE Trans. Circuits Syst. Video Technol.*, vol. 13, no. 7, pp. 560–576, Jul. 2003.

[2] G. J. Sullivan, J.-R. Ohm, W.-J. Han, and T. Wiegand, "Overview of the high efficiency video coding (HEVC) standard," *IEEE Trans. Circuits Syst. Video Technol.*, vol. 22, no. 12, pp. 1649–1668, Dec. 2012.

[3] D. Flynn, D. Marpe, M. Naccari, T. Nguyen, C. Rosewarne, K. Sharman, J. Sole, and J. Xu, "Overview of the range extensions for the HEVC standard: Tools, profiles, and performance," *IEEE Trans. Circuits Syst. Video Technol.*, vol. 26, no. 1, pp. 4–19, Jan. 2016.

[4] J. A. Ferwerda, "Elements of early vision for computer graphics," *IEEE Comput. Graph. Appl.*, vol. 21, no. 4, pp. 22–33, Sep. 2001.

[5] R. K. Chaurasiya and V. Chourasia, "High dynamic range imaging for dynamic scenes," in *Proc. 4th Int. Conf. Commun. Syst. Netw. Technol.*, Scottsdale, AZ, USA, Apr. 2014, pp. 337–442.

[6] T. Smith and J. Guild, "The C.I.E. Colorimetric standards and their use," *Trans. Opt. Soc.*, vol. 33, no. 3, pp. 73–134, Jan. 1931.

[7] *Parameter Values for the HDTV standards for Production and International Programme Exchange*, Standard Recommendation ITU-R BT.709-5, ITU-T, Apr. 2002. [Online]. Available: http://www.itu.int/rec/R-REC-BT.709

[8] *Parameter Values for Ultra-High Definition Television Systems for Production and International Programme Exchange*, Standard Recommendation ITU-R BT.2020-1, ITU-T, Jun. 2014. [Online]. Available: http://www.itu.int/rec/R-REC-BT.2020

[9] K. Jansen. (Feb. 2014). The Pointer's Gamut—The Coverage of Real Surface Colors by RGB Color Spaces and Wide Gamut Displays. TFT Central. [Online]. Available: http://www.tftcentral.co.uk/articles/pointers_gamut.htm

[10] J. Samuelsson, C. Fogg, A. Norkin, A. Segall, J. Sträöm, G. Sullivan, P. Topiwala, and A. Tourapis, *Conversion and Coding Practices for HDR/WCG Y'CbCr 4:2:0 Video with PQ Transfer Characteristics (Draft 4)*, document JCTVC-Z1017, 26th Meeting, Geneva, Switzerland, Jan. 2017.

[11] P. Bjäörkman, "The Ultra HD equation," *EBU Tech-I J.*, no. 17, p. 9, Sep. 2013. [Online]. Available: https://tech.ebu.ch/docs/tech-i/ebu_tech-i_017.pdf

[12] "Understanding ultra high definition television: Technologies for enhanced viewing experiences," Ericsson, Stockholm, Sweden, White Paper Uen 284 23-3266, Nov. 2015. [Online]. Available: http://www.dutchguild.nl/02feb16/wp-uhd-update-v3.pdf

[13] E. Francois, C. Fogg, Y. He, X. Li, A. Luthra, and A. Segall, "High dynamic range and wide color gamut video coding in HEVC: Status and potential future enhancements," *IEEE Trans. Circuits Syst. Video Technol.*, vol. 26, no. 1, pp. 63–75, Jan. 2016.

[14] *Reference Electro-Optical Transfer Function for Flat Panel Displays Used in HDTV Studio Production*, Standard Recommendation ITU-R BT.1886, ITU-T, Mar. 2011. [Online]. Available: http://www.itu.int/rec/R-REC-BT.1886

[15] M. Yuen and H. R. Wu, "A survey of hybrid MC/DPCM/DCT video coding distortions," *Signal Process.*, vol. 70, no. 3, pp. 247–278, Nov. 1998.

[16] A. N. Netravali and B. G. Haskell, *Digital Pictures: Representation and Compression*. New York, NY, USA: Plenum Press, 1988.

[17] K. Zeng, T. Zhao, A. Rehman, and Z. Wang, "Characterizing perceptual artifacts in compressed video streams," *Proc. SPIE*, vol. 9014, Feb. 2014, Art. no. 90140Q.

[18] H. R. Wu, M. Yuen, and B. Qiu, "Video coding distortion classification and quantitative impairment metrics," in *Proc. 3rd Int. Conf. Signal Process. (ICSP)*, Beijing, China, Oct. 1996, vol. 2, pp. 962–965.

[19] S. E. Susstrunk and S. Winkler, "Color image quality on the Internet," *Proc. SPIE*, vol. 5304, pp. 118–131, Dec. 2003.

[20] A. Punchihewa and J. Armstrong, "Effects of sub-sampling and quantisation on colour bleeding due to image and video compression," in *Proc. 23rd Int. Conf. Image Vis. Comput.*, Wellington, New Zealand, Nov. 2008, pp. 1–6.

[21] G. Spampinato, A. Castorina, A. Bruna, and A. Capra, "JPEG adaptive chromatic post-processing," in *Proc. 14th Int. Conf. Image Anal. Process.-Workshops (ICIAPW)*, Modena, Italy, Sep. 2007, pp. 202–205.

[22] G. K. Wallace, "The JPEG still picture compression standard," *IEEE Trans. Consum. Electron.*, vol. 38, no. 1, pp. 18–34, Feb. 1992.

[23] F.-X. Coudoux, M. Gazalet, and P. Corlay, "An adaptive postprocessing technique for the reduction of color bleeding in DCT-coded images," *IEEE Trans. Circuits Syst. Video Technol.*, vol. 14, no. 1, pp. 114–121, Jan. 2004.

[24] S. Li, O. C. Au, L. Sun, W. Dai, and R. Zou, "Color bleeding reduction in image and video compression," in *Proc. Int. Conf. Comput. Sci. Netw. Technol.*, Dec. 2011, pp. 665–669.

[25] Y. Zhang, E. Reinhard, and D. Bull, "Perception-based high dynamic range video compression with optimal bit-depth transformation," in *Proc. 18th IEEE Int. Conf. Image Process.*, Sep. 2011, pp. 1321–1324.

[26] Y. Zhang, D. Agrafiotis, M. Naccari, M. Mrak, and D. R. Bull, "Visual masking phenomena with high dynamic range content," in *Proc. IEEE Int. Conf. Image Process.*, Sep. 2013, pp. 2284–2288.

[27] Y. Zhang, M. Naccari, D. Agrafiotis, M. Mrak, and D. R. Bull, "High dynamic range video compression by intensity dependent spatial quantization in HEVC," in *Proc. Picture Coding Symp. (PCS)*, 2013, pp. 353–356.

[28] Y. Zhang, M. Naccari, D. Agrafiotis, M. Mrak, and D. R. Bull, "High dynamic range video compression exploiting luminance masking," *IEEE Trans. Circuits Syst. Video Technol.*, vol. 26, no. 5, pp. 950–964, May 2016.

[29] T. Lu, F. Pu, P. Yin, T. Chen, and W. Husak, "Implication of high dynamic range and wide color gamut content distribution," *Proc. SPIE*, vol. 9599, Sep. 2015, Art. no. 95990B, doi: 10.1117/12.2188572.

[30] X. Xiu, P. Hanhart, R. Vanam, Y. He, Y. Ye, T. Lu, F. Pu, P. Yin, W. Husak, and T. Chen, *Description of SDR, HDR, and 360 Video Coding Technology Proposal by Inter Digital Communications and Dolby Laboratories*, document JVET-J0015, 10th Meeting, San Diego, CA, USA, Apr. 2018.

[31] Y. Cheng, W.-J. Chien, H.-C. Chuang, M. Coban, J. Dong, H. E. Egilmez, N. Hu, M. Karczewicz, A. Ramasubramanian, D. Rusanovskyy, A. Said, V. Seregin, G. Van Der Auwera, K. Zhang, L. Zhang, P. Bordes, Y. Chen, C. Chevance, E. Francois, F. Galpin, F. Le Leannec, K. Naser, T. Poirier, F. Racape, G. Rath, A. Robert, F. Urban, T. Viellard, *Description of SDR, HDR and 360° Video Coding Technology Proposal by Qualcomm and Technicolor—Low and High Complexity Versions*, document JVET-J0021, 10th Meeting, San Diego, CA, USA, Apr. 2018.

[32] J. Strom, J. Samuelsson, and K. Dovstam, "Luma adjustment for high dynamic range video," in *Proc. Data Compress. Conf. (DCC)*, Mar. 2016, pp. 319–328.

[33] J. Samuelsson, M. Petersson, J. Strom, and K. Andersson, *Using Chroma QP Offset on HDR Sequences*, Standard ISO/IEC JTC 1/SC 29/WG11 MPEG2015/m36581, Warsaw, Poland, Jun. 2015.

[34] J. Strom, K. Andersson, M. Pettersson, P. Hermansson, J. Samuelsson, A. Segall, J. Zhao, S.-H. Kim, K. Misra, A. M. Tourapis, Y. Su, and D. Singer, "High quality HDR video compression using HEVC main 10 profile," in *Proc. Picture Coding Symp. (PCS)*, Dec. 2016, pp. 1–5.

[35] M.-S. Li, M.-J. Chen, K.-H. Tai, and K.-L. Sue, "Fast mode decision based on human noticeable luminance difference and rate distortion cost for H.264/AVC," *EURASIP J. Adv. Signal Process.*, vol. 2013, no. 1, p. 60, Dec. 2013, doi: 10.1186/1687-6180-2013-60.

[36] Z. Wang, A. C. Bovik, H. R. Sheikh, and E. P. Simoncelli, "Image quality assessment: From error visibility to structural similarity," *IEEE Trans. Image Process.*, vol. 13, no. 4, pp. 600–612, Apr. 2004.

[37] Z. Chen and C. Guillemot, "Perceptually-friendly H.264/AVC video coding based on foveated Just-Noticeable-Distortion model," *IEEE Trans. Circuits Syst. Video Technol.*, vol. 20, no. 6, pp. 806–819, Jun. 2010.

[38] *HEVC Test Model (HM)-HEVC Reference Software*. Accessed: Mar. 10, 2020. [Online]. Available: http://hevc.hhi.fraunhofer.de/svn/svn_HEVCSoftware/

[39] E. Francois, J. Sole, J. Strom, and P. Yin, *Common Test Conditions for HDR/WCG Video Coding Experiment*, document JCTVC-W1020, 23rd JCT-VC Meeting, San Diego, CA, USA, Feb. 2016.

[40] M. Narwaria, M. Perreira Da Silva, and P. Le Callet, "HDR-VQM: An objective quality measure for high dynamic range video," *Signal Process., Image Commun.*, vol. 35, pp. 46–60, Jul. 2015.

[41] *Subjective Video Quality Assessment Methods for Multimedia Applications*, Standard Recommendation ITU-T P.910, P. ITU-T recommendation, Apr. 2008.

[42] R. Mantiuk, K. Kim, G. Allan Rempel, and W. Heidrich, "HDR-VDP-2: A calibrated visual metric for visibility and quality predictions in all luminance conditions," *ACM Trans. Graph.*, vol. 30, no. 4, pp. 1–4, 2011.

[43] M. Narwaria, R. K. Mantiuk, M. P. Da Silva, and P. Le Callet, "HDR-VDP-2.2: A calibrated method for objective quality prediction of high-dynamic range and standard images," *J. Electron. Imag.*, vol. 24, no. 1, Jan. 2015, Art. no. 010501, doi: 10.1117/1.jei.24.1.010501.

JONG-HYEOK LEE received the B.S. and M.S. degrees in computer engineering, in 2011 and 2013, respectively, and the Ph.D. degree in computer and electronics convergence engineering from Sun Moon University, South Korea, in 2019.

In 2015, he joined the Realistic Broadcasting Media Research Team, Electronics and Telecommunications Research Institute (ETRI). From 2016 to 2018, he joined the Big Data Research Center, Sookmyung Women's University, where he was a Visiting Researcher. In 2019, he joined the Research and Development Team, PIXTREE Inc., Seoul, South Korea, where he is currently a Senior Researcher. His research interests include video compression, real-time processing, and deep learning-based video restoration.

YOUNG-WOON LEE received the B.S. and M.S. degrees in computer engineering from Sun Moon University, in 2016 and 2018, respectively, where he is currently pursuing the Ph.D. degree in computer and electronics convergence engineering.

His research interests include video signal processing, machine learning, and deep learning-based video compression.

DONGSAN JUN received the B.S. degree in electrical engineering and computer science from Pusan National University, South Korea, in 2002, and the M.S. and Ph.D. degrees in electrical engineering from the Korea Advanced Institute of Science and Technology (KAIST), Daejeon, South Korea, in 2004 and 2011, respectively.

In 2004, he joined the Realistic AV Research Group, Electronics and Telecommunications Research Institute (ETRI), Daejeon, where he was a Principal Researcher. In March 2018, he joined the Department of Information and Communication Engineering, Kyungnam University, Changwon, South Korea, where he is currently an Assistant Professor. His research interests include image/video computing systems, pattern recognition, video compression, real-time processing, and realistic broadcasting systems.

BYUNG-GYU KIM (Senior Member, IEEE) received the B.S. degree from Pusan National University, South Korea, in 1996, the M.S. degree from the Korea Advanced Institute of Science and Technology (KAIST), in 1998, and the Ph.D. degree from the Department of Electrical Engineering and Computer Science, KAIST, in 2004.

In March 2004, he joined the Real-Time Multimedia Research Team, Electronics and Telecommunications Research Institute (ETRI), South Korea, where he was a Senior Researcher. In ETRI, he developed so many real-time video signal processing algorithms and patents and received the Best Paper Award, in 2007. From February 2009 to February 2016, he was an Associate Professor with the Division of Computer Science and Engineering, Sun Moon University, South Korea. In March 2016, he joined the Department of Information Technology (IT) Engineering, Sookmyung Women's University, South Korea, where he is currently a Full Professor. He has published over 240 international journal articles and conference papers, patents in his field. His research interests include image and video signal processing for the content-based image coding, video coding techniques, 3D video signal processing, deep/reinforcement learning algorithm, embedded multimedia systems, and intelligent information system for image signal processing.

Dr. Kim is a Professional Member of ACM and IEICE. He also served or serves on Organizing Committee of CSIP 2011, a Co-Organizer of CICCAT2016/2017, The Seventh International Conference on Advanced Computing, Networking, and InformaticsN (ICACNI2019), the EAI 13-th International Conference on Wireless Internet Communications Conference (WiCON 2020), and the Program Committee Members of many international conferences. He has received the Special Merit Award for Outstanding Paper from the IEEE Consumer Electronics Society, at IEEE ICCE 2012, the Certification Appreciation Award from the SPIE Optical Engineering, in 2013, and the Best Academic Award from the CIS, in 2014. He has been honored as an IEEE Senior Member, in 2015. He has been serving as a Professional Reviewer in many academic journals, including IEEE, ACM, Elsevier, Springer, Oxford, SPIE, IET, MDPI, IT&T, and so on. In 2007, he has served as an Editorial Board Member for the *International Journal of Soft Computing*, *Recent Patents on Signal Processing*, the *Research Journal of Information Technology*, the *Journal of Convergence Information Technology*, and the *Journal of Engineering and Applied Sciences*. He has been serving as an Associate Editor for *Circuits, Systems and Signal Processing* (Springer), *The Journal of Supercomputing* (Springer), *The Journal of Real-Time Image Processing* (Springer), *Heliyon-Computer Science* (Cell press), and *Applied Sciences* (MDPI). Since March 2018, he has been serving as the Editor-in-Chief for *The Journal of Multimedia Information System* and an Associate Editor for IEEE Access Journal. He has been serving as a Topic Editor for *Sensors and Electronics* (MDPI).

• • •